Astronomy & Astrophysics

LETTER TO THE EDITOR

Augmenting the power of time-delay cosmography in lens galaxy clusters by probing their member galaxies

II. Cosmic chronometers

P. Bergamini[1,2], S. Schuldt[1,3], A. Acebron[1,3], C. Grillo[1,3], U. Meštrić[1,2], G. Granata[1,3], G. B. Caminha[4,5], M. Meneghetti[2], A. Mercurio[6,7,8], P. Rosati[9,2], S. H. Suyu[4,5,10], and E. Vanzella[2]

[1] Dipartimento di Fisica, Università degli Studi di Milano, Via Celoria 16, 20133 Milano, Italy
    e-mail: `pietro.bergamini@unimi.it`
[2] INAF – OAS, Osservatorio di Astrofisica e Scienza dello Spazio di Bologna, Via Gobetti 93/3, 40129 Bologna, Italy
[3] INAF – IASF Milano, Via A. Corti 12, 20133 Milano, Italy
[4] Technical University of Munich, TUM School of Natural Sciences, Department of Physics, James-Franck-Str 1, 85748 Garching, Germany
[5] Max-Planck-Institut für Astrophysik, Karl-Schwarzschild-Str. 1, 85748 Garching, Germany
[6] Universitá di Salerno, Dipartimento di Fisica "E.R. Caianiello", Via Giovanni Paolo II 132, 84084 Fisciano, (SA), Italy
[7] INAF – Osservatorio Astronomico di Capodimonte, Via Moiariello 16, 80131 Napoli, Italy
[8] INFN – Gruppo Collegato di Salerno – Sezione di Napoli, Dipartimento di Fisica "E.R. Caianiello", Universitá di Salerno, Via Giovanni Paolo II, 132, 84084 Fisciano, (SA), Italy
[9] Dipartimento di Fisica e Scienze della Terra, Università degli Studi di Ferrara, Via Saragat 1, 44122 Ferrara, Italy
[10] Academia Sinica Institute of Astronomy and Astrophysics (ASIAA), 11F of ASMAB, No.1, Section 4, Roosevelt Road, Taipei 10617, Taiwan

ABSTRACT

We present a novel approach to measuring the expansion rate and the geometry of the Universe, which combines time-delay cosmography in lens galaxy clusters with pure samples of 'cosmic chronometers' by probing the member galaxies. The former makes use of the measured time delays between the multiple images of time-varying sources strongly lensed by galaxy clusters, while the latter exploits the most massive and passive cluster member galaxies to measure the differential time evolution of the Universe. We applied two different statistical techniques, adopting realistic errors on the measured quantities, to assess the accuracy and the gain in precision on the values of the cosmological parameters. We demonstrate that the proposed combined method allows for a robust and accurate measurement of the value of the Hubble constant. In addition, this provides valuable information on the other cosmological parameters thanks to the complementarity between the two different probes in breaking parameter degeneracies. Finally, we showcased the immediate observational feasibility of the proposed joint method by taking advantage of the existing high-quality spectro-photometric data for several lens galaxy clusters.

Key words. gravitation – gravitational lensing: strong – methods: data analysis – galaxies: clusters: general – galaxies: clusters: individual: MACS J1149.5+2223 – cosmological parameters

1. Introduction

Emergent, independent probes for measuring the present-day expansion rate, defined as the Hubble constant (H_0), and the geometry of the Universe can offer valuable insights into unknown systematic effects and help clarify current tensions in cosmology (Verde et al. 2019; Moresco et al. 2022). Time-delay cosmography (TDC) grants such an opportunity. Almost sixty years after Refsdal (1964)'s original idea that strongly lensed supernovae (SNe) with measured time delays between their multiple images could offer a novel way to measure the value of H_0, this technique has provided competitive estimates of its value (e.g. Suyu et al. 2017; Treu & Marshall 2016; Grillo et al. 2018; Birrer et al. 2019; Wong et al. 2020; Shajib et al. 2023).

Using time-varying sources strongly lensed by galaxy clusters represents a complementary and powerful avenue.

The multiply-imaged SN 'Refsdal' in the galaxy cluster MACS J1149.5+2223 (hereafter, MACS 1149, e.g. Lotz et al. 2017) has allowed for the first measurement of the value of H_0 via a multiply-imaged SN with measured time delays (Kelly et al. 2016, 2023). In particular, Grillo et al. (2018, 2020), using a full strong lensing analysis, inferred the value of H_0 with a 6% total (statistical plus systematic) uncertainty. In this series of two Letters, we present novel methods to enhance and complement the power of TDC in lens galaxy clusters, first by observing Type Ia Supernovae (SNe Ia) in cluster member galaxies (Acebron et al. 2023, Letter I, hereafter) and then by using a subset of member galaxies in lens galaxy clusters as 'cosmic chronometers' (CCs).

As shown in Grillo et al. (2018, 2020), to take full advantage of lens clusters as cosmological probes, it is necessary to construct an accurate cluster total mass model by

leveraging extensive high-quality spectro-photometric datasets (e.g. Caminha et al. 2017; Bergamini et al. 2019; Lagattuta et al. 2023; Acebron et al. 2022b). In parallel, these data (already available for several lens galaxy clusters) enable us to homogeneously select pure samples of red, massive, and passive cluster members and exploit them as CCs (Jimenez & Loeb 2002; Stern et al. 2010a). In this work, we explore, for the first time, the idea of taking advantage of some member galaxies as CCs to yield an independent measurement of the value of the Hubble parameter at the lens cluster redshift. From the combination of these two cosmological probes, we can then assess the gain in precision on the measurement of the values of the main cosmological parameters.

The Letter is organised as follows. In Sect. 2, we concisely illustrate the principles of the TDC and CC probes to infer the values of the cosmological parameters. In Sect. 3, we detail our methods to quantify the precision attainable in these measurements with the proposed joint technique. In Sect. 4, we present our results and describe the observational feasibility of carrying out this analysis. Finally, we draw our conclusions in Sect. 5.

2. Methods

In this section, we summarise the basic principles behind the TDC and CC techniques used to measure the values of H_0, the present-day cosmological densities of matter (Ω_m) and dark energy (Ω_de), and the dark-energy equation of state parameter (w).

2.1. Time-delay cosmography

Gravitational lensing refers to the effect according to which the light rays emitted from a background source are deflected by a foreground mass distribution, such as a galaxy or a galaxy cluster. When the total mass density of the gravitational lens is sufficiently high, we reach the strong-lensing regime and lensed sources are multiply imaged.

If the luminosity of a background source is intrinsically variable in time, such as that of quasars or SNe, its different multiple images appear with a delay in time to the observer that can be estimated. In particular, the time delay,

$$\Delta t_{i_1 i_2} = \frac{D_{\Delta t}}{c} \Delta \phi_{i_1 i_2}, \tag{1}$$

between two images, i_1 and i_2, of the same background source can be measured through dedicated (photometric) monitoring campaigns (e.g. Courbin et al. 2018; Millon et al. 2020; Kelly et al. 2023), while the Fermat potential, ϕ, is obtained by modelling the total mass distribution of the gravitational lens (c is the speed of light). By determining these two quantities, one can probe the so-called time-delay distance, $D_{\Delta t}$ (Suyu et al. 2010), defined as

$$D_{\Delta t} = (1 + z_\mathrm{d}) \frac{D_\mathrm{d}^\mathrm{A} D_\mathrm{s}^\mathrm{A}}{D_\mathrm{ds}^\mathrm{A}}, \tag{2}$$

where z_d is the redshift of the gravitational lens and D_d^A, D_s^A, and D_ds^A are the angular-diameter distances to the lens, to the source, and between the lens and the source, respectively. From this combination of distances, we see that $D_{\Delta t}$ is proportional to H_0^{-1}, with a weaker dependence on the values of the other cosmological parameters (Ω_m, Ω_de, and w). The typical relative total (statistical plus systematic) errors on the value of $D_{\Delta t}$ achieved

by using a single (galaxy or cluster) gravitational lens range from ~4% to ~9% (e.g. Suyu et al. 2014; Birrer et al. 2019; Grillo et al. 2020; Wong et al. 2020; Shajib et al. 2023).

2.2. Cosmic chronometers

The CC technique, introduced by Jimenez & Loeb (2002), is designed to probe the cosmic expansion history of the Universe, $H(z)$, independently from the adopted cosmological model. The CC approach exploits a time-redshift relation which, from the definition of $H(z)$ and those of the scale factor and redshift within a Friedmann-Robertson-Walker metric, can be expressed as

$$H(z) = -\frac{1}{1+z} \frac{\mathrm{d}z}{\mathrm{d}t}, \tag{3}$$

where $\mathrm{d}t$ is the differential time evolution of the Universe in a given redshift interval, $\mathrm{d}z$. The latter can be robustly measured from spectroscopy, while $\mathrm{d}t$ can be determined by using a homogeneous population of objects, in different redshift bins, as CCs. Here, $H(z)$ can be expressed as a function of redshift and of the values of the cosmological parameters, $H(z; H_0, \Omega_\mathrm{m}, \Omega_\mathrm{de}, w)$, scaling proportionally with the value of H_0 and with a weaker dependence on the other cosmological parameters.

Extremely massive and passively evolving galaxies, both in blank and cluster fields, have been identified as optimal CCs (e.g. Stern et al. 2010a; Moresco et al. 2012; Zhang et al. 2014). One of the key steps in this technique is the selection of a pure sample of such CCs, for which a combination of photometric and spectroscopic criteria is commonly adopted (see Moresco et al. 2022, for a review). In particular, spectroscopy is crucial to ensure the absence of residual emission lines, which can imply the existence of ongoing star formation. Typically, high stellar-mass or stellar velocity-dispersion cuts are also applied to select the most massive galaxies. The age of the selected CCs can be estimated following different techniques, such as a full spectral-fitting approach (e.g. Simon et al. 2005; Stern et al. 2010a; Zhang et al. 2014; Ratsimbazafy et al. 2017), the analysis of specific features of the galaxy spectrum, known as Lick indices (e.g. Borghi et al. 2022b,a), or of the rest-frame 4000 Å break (e.g. Moresco et al. 2012; Moresco 2015). The total error budget on the measurement of the age of the CCs includes the contributions from several factors, such as residual star-forming contaminants, adopted stellar population synthesis models, and stellar metallicity estimates. With this method, the current precision on the value of $H(z)$ ranges from ~10% to ~20% (see Table 1 in Moresco et al. 2022).

3. Simulations

In this section, we describe our simulation techniques exploiting two different approaches: one Bayesian and one Monte Carlo. As in Letter I, we consider MACS 1149, located at $z_\mathrm{d} = 0.54$, as our reference lens cluster (Grillo et al. 2016; Treu et al. 2016; Lotz et al. 2017). The time-varying multiply-imaged source, a Type II SN known as SN 'Refsdal', is at $z_\mathrm{s} = 1.49$ (Kelly et al. 2015, 2016). By measuring the value of the Hubble parameter at the effective redshift of MACS 1149 (see Sect. 4), we obtain $H(z) = H(z_\mathrm{d})$.

The Bayesian method assumes the following general form for the likelihood function associated with the two different probes i, namely, TDC and CC:

$$\mathcal{L}_i = \frac{1}{\sigma_i \sqrt{2\pi}} \exp(-\chi_i^2/2), \tag{4}$$

Table 1. Intervals at the 68% confidence level for the values of the cosmological parameters obtained with the Bayesian method.

Err. [b] $D_{\Delta t}$	Err. [b] $H(z_{\rm d})$	Flat-ΛCDM [a]		Open-wCDM			
		H_0 [c]	$\Omega_{\rm m}$	H_0 [c]	$\Omega_{\rm m}$	$\Omega_{\rm de}$	w
5%	10%	$69.4^{+3.8}_{-3.6}$	$0.33^{+0.19}_{-0.15}$	$69.9^{+6.5}_{-5.5}$	$0.43^{+0.36}_{-0.31}$	$0.71^{+0.19}_{-0.29}$	$-1.18^{+0.55}_{-0.55}$
5%	20%	$69.0^{+3.9}_{-3.6}$	$0.40^{+0.31}_{-0.24}$	$69.8^{+6.3}_{-5.3}$	$0.45^{+0.36}_{-0.31}$	$0.58^{+0.28}_{-0.34}$	$-1.14^{+0.65}_{-0.59}$
10%	10%	$68.9^{+7.5}_{-6.6}$	$0.33^{+0.24}_{-0.17}$	$68.1^{+9.3}_{-7.1}$	$0.41^{+0.36}_{-0.29}$	$0.65^{+0.23}_{-0.32}$	$-1.18^{+0.59}_{-0.56}$
10%	20%	$68.9^{+7.4}_{-6.3}$	$0.39^{+0.32}_{-0.24}$	$69.1^{+9.0}_{-7.2}$	$0.44^{+0.36}_{-0.31}$	$0.58^{+0.28}_{-0.35}$	$-1.13^{+0.66}_{-0.60}$

Notes. [a]$\Omega_{\rm m} + \Omega_{\rm de} = 1$ and $w = -1$. [b]Adopted percentage relative errors. [c](km s^{-1} Mpc^{-1}).

where

$$\chi^2_{\rm TDC} = \left(\frac{D_{\Delta t,\,{\rm true}} - \hat{D}_{\Delta t}}{\sigma_{D_{\Delta t,\,{\rm true}}}}\right)^2 \quad {\rm and} \quad \chi^2_{\rm CC} = \left(\frac{H_{\rm true}(z_{\rm d}) - \hat{H}(z_{\rm d})}{\sigma_{H_{\rm true}(z_{\rm d})}}\right)^2,$$

(5)

for the TDC and CC methods, respectively. In these equations, $D_{\Delta t,\,{\rm true}}$ and $H_{\rm true}(z_{\rm d})$ are the values of the time-delay distance and of the Hubble parameter (at the redshift of the considered lens cluster, $z_{\rm d}$) computed in the fiducial input cosmological model that assumes $H_0 = 70$ km s^{-1} Mpc^{-1}, $\Omega_{\rm m} = 0.3$, $\Omega_{\rm de} = 0.7$, and $w = -1$. The quantities $\hat{D}_{\Delta t}$ and $\hat{D}^{\rm L}$ correspond to these distances obtained by sampling the two-dimensional (H_0, $\Omega_{\rm m}$) or four-dimensional (H_0, $\Omega_{\rm m}$, $\Omega_{\rm de}$, w) parameter space (considering $z_{\rm d} = 0.54$ and $z_{\rm s} = 1.49$). Here, we adopt realistic errors on the relevant quantities $D_{\Delta t}$ and $H(z)$, namely, $\sigma_{D_{\Delta t,{\rm true}}}$ and $\sigma_{H_{\rm true}(z_{\rm d})}$, ranging from 5% to 10% and from 10% to 20%, respectively. In this work, we adopt these intervals to represent different scenarios. The total likelihood function accounting for the combination of the two techniques is obtained by multiplying the individual likelihood functions of each method as

$$\mathcal{L}_{\rm tot} = \mathcal{L}_{\rm TDC} \times \mathcal{L}_{\rm CC}.$$

(6)

In order to define the parameter posterior distributions, the following flat priors are assumed on the values of the cosmological parameters: $H_0 \in [20, 120]$ km s^{-1} Mpc^{-1}, $\Omega_{\rm m}$ and $\Omega_{\rm de} \in [0, 1]$, and $w \in [-2, 0]$. The final log-posterior distributions are sampled by using emcee, which is the Python implementation of the affine-invariant Markov chain Monte Carlo (MCMC) ensemble sampler (Goodman & Weare 2010; Foreman-Mackey et al. 2013). We performed our analysis adopting a flat-Λcold dark matter (CDM) ($\Omega_{\rm m} + \Omega_{\rm de} = 1$ and $w = -1$) or an open-wCDM cosmological model. The two- (H_0, $\Omega_{\rm m}$) and four-dimensional (H_0, $\Omega_{\rm m}$, $\Omega_{\rm de}$, w) parameter space is then explored by using ten walkers, performing 10^5 steps each. We note that the first 5000 steps of the walkers are removed as the burn-in phase, which corresponds to ~100 times the integrated auto-correlation time of the parameters.

Differently, in the Monte Carlo approach, we extracted 10^6 realisations of $D_{\Delta t}$ and $H(z_{\rm d})$ from Gaussian distributions centred on the values of $D_{\Delta t,\,{\rm true}}$ and $H_{\rm true}(z_{\rm d})$ (see above) and with standard deviations corresponding to the errors reported in Table 1. Subsequently, by considering a two- (H_0, $\Omega_{\rm m}$) or a four-dimensional (H_0, $\Omega_{\rm m}$, $\Omega_{\rm de}$, w) grid divided into 1000 equally spaced bins and covering the assumed prior intervals, we computed the values of $D_{\Delta t}$ and $H(z_{\rm d})$ for each possible combination of cosmological parameters (corresponding to the different grid points). Finally, we determined the combination of cosmological parameter values that best reproduces each of the 10^6 simu-

lated measurements by computing the χ^2 functions corresponding to the TDC and CC techniques, separately and combined (see Eq. (5)).

Both simulation methods yield median values of the cosmological parameters and associated precision in excellent agreement, proving the robustness of our analysis. Given that the Bayesian approach is more efficient and robust in sampling the posterior distribution, especially in a high-dimensional parameter space (Wolz et al. 2012), we present in the following only the results obtained with this technique.

4. Discussion

Table 1 summarises the median values and the 1σ confidence intervals of the cosmological parameters within the adopted cosmological models and assuming different values for the uncertainties on $D_{\Delta t}$ and $H(z_{\rm d})$. In the left panel of Fig. 1, we show, in a flat-ΛCDM model, the marginalised posterior probability distributions and the 1, 2, and 3σ confidence regions for H_0 and $\Omega_{\rm m}$ inferred from the TDC (blue) and the CC (orange) techniques, and their combination (black), when assuming a 5% and 10% relative error for each technique, respectively. In the right panel of the same figure, we also assess the improvement of the precision on the values of these cosmological parameters from the combination of the TDC and CC techniques with an independent SN Ia luminosity distance ($D^{\rm L}$) measurement in a cluster member galaxy, as newly proposed in Letter I. This is done by including an additional $\mathcal{L}_{\rm SNIa}$ term (where the corresponding $\chi^2_{\rm SNIa}$ is defined in Eq. (6) in Letter I and a 5% relative uncertainty on the value of $D^{\rm L}$ is assumed) in Eq. (6). We note that the uncertainty on H_0 is always driven by that of the term $D_{\Delta t}$. This is also shown by the fact that, for a fixed value of $\sigma_{D_{\Delta t}}$, considering more- or less- conservative relative errors on $H(z_{\rm d})$ (see Table 1) or $D^{\rm L}$ (see Letter I) yields a similar precision on the measurement of H_0. When considering the more general open-wCDM model, its value is still robustly measured, with a slightly larger posterior probability distribution than in the flat-ΛCDM model. This result demonstrates that the estimate of H_0 is only mildly dependent on the assumed cosmological model.

As discussed in Sect. 2 and in Letter I, the three techniques are more sensitive to the value of H_0 than to those of the other cosmological parameters. For instance, the marginalised posterior probability distribution functions of $\Omega_{\rm m}$ are flat when considering each method alone. Remarkably, their combination allows for an estimate of the value of $\Omega_{\rm m}$ (with a significant statistical error, between ~50% and ~70% for more or less conservative scenarios; see Table 1). This can be explained by the orientations of the H_0–$\Omega_{\rm m}$ intrinsic degeneracy from the different cosmological probes. In particular, the H_0–$\Omega_{\rm m}$ degeneracies from the TDC and CC techniques are oriented in different
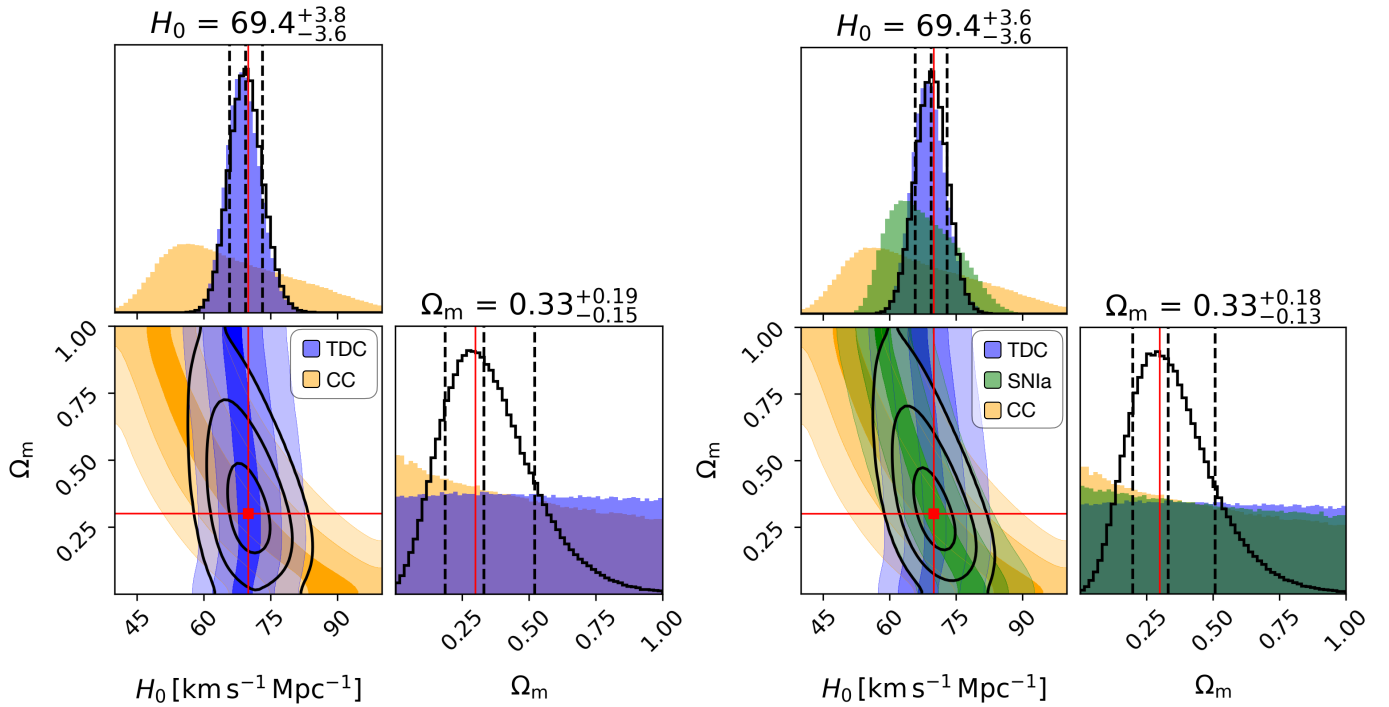
Fig. 1. Inferred values for the cosmological parameters H_0 and $\Omega_{\rm m}$ in a flat-ΛCDM model, assuming a total relative uncertainty of 5%, 10%, and 5% for $D_{\Delta t}$, $H(z)$, and $D^{\rm L}$, respectively (we fixed $z_{\rm d} = 0.54$, $z_{\rm s} = 1.49$, and $z_{\rm SNIa} = 0.54$). The marginalised posterior distributions for the TDC, CC, and SNIa techniques are shown in blue, orange, and green, respectively. The total marginalised posterior distributions (black) obtained by combining the TDC and CC, and TDC, CC, and SNIa methods are shown in the left and right panels, respectively. The 16th, 50th, and 84th percentiles of the combined marginalised distributions are highlighted with vertical dashed lines and the associated values are reported. The fiducial values are marked in red. The contour levels on the planes represent the 1, 2, and 3σ confidence regions.

directions, such that the overlapping region is smaller than for the joint TDC and SN Ia method. Thus, when considering the most optimistic scenario in the flat-ΛCDM model, the combined TDC and CC technique yields improved measurements of H_0 and $\Omega_{\rm m}$ by about a factor of $\sim$1.06 and $\sim$1.22, respectively, compared to the joint TDC and SN Ia method (see Letter I). However, since the degeneracy between H_0 and $\Omega_{\rm m}$ from the SN Ia method lies in between that from the TDC and CC methods, the gain in precision from the combination of the three probes is negligible. We also highlight that the measured values of the cosmological parameters and, in particular, that of H_0, obtained by combining two or three of the discussed techniques (TDC, CC, and SNIa) are always accurately recovered (see Table 1).

This is a conservative estimate of the value of $\Omega_{\rm m}$, since (for simplicity) we are neglecting the contribution of the family-ratio term. This quantity can be probed when large samples of multiple images at different redshifts are observed, as is the case in lens galaxy clusters (e.g. Caminha et al. 2016; Richard et al. 2021; Bergamini et al. 2023a). Thus, the values of $\Omega_{\rm m}$, $\Omega_{\rm de}$, and w can also be measured (Jullo et al. 2010; Linder 2011; Grillo et al. 2018; Caminha et al. 2022).

After illustrating the possibility of enhancing and complementing the TDC technique with the combination of an estimate of $H(z_{\rm d})$ from exploiting the most massive cluster member galaxies as CCs, we discuss the observational feasibility of implementing the proposed joint method. Multiple studies suggest that early-type cluster galaxies have assembled most of their stellar mass through massive star-formation events at early cosmic times (Bernardi et al. 1998; Gobat et al. 2008; Ferré-Mateu et al. 2014; Khullar et al. 2022), with little star formation happening thereafter (Treu et al. 2005; Thomas et al. 2005). Such objects

constitute thus a very homogeneous population, which is illustrated by the observation of a tight red sequence in the colour-magnitude diagram (Faber et al. 1987; Gladders & Yee 2000; De Lucia et al. 2007), being already in place at high redshifts (e.g. Gobat et al. 2008; Menci et al. 2008; Lidman et al. 2008; Hilton et al. 2009; Cerulo et al. 2016; Strazzullo et al. 2016). Galaxy clusters are thus unique environments in which to exploit the old and homogeneous population of massive, early-type galaxies as CCs (Stern et al. 2010a,b).

Several lens galaxy clusters count with extensive, high-quality spectro-photometric data that can be readily exploited to select high-purity samples of CC tracers. In particular, high-resolution, deep, multi-band imaging of cluster fields, spanning the near-ultraviolet to the near-infrared (Postman et al. 2012; Lotz et al. 2017; Estrada et al. 2023), is valuable for distinguishing star-forming and passive populations (Moresco et al. 2022). Thanks to its powerful capabilities, the Multi Unit Spectroscopic Explorer (MUSE, Bacon et al. 2012) integral-field spectrograph, on the Very Large Telescope (VLT), is the ideal instrument for carrying out spectroscopic studies of galaxies residing in galaxy cluster cores. With a fairly large field of view ($\sim$1 arcmin^2), MUSE has high spatial sampling (0.2″ px^{-1}), relatively high spectral resolution ($R \sim 3000$), and large wavelength coverage (4750–9350 Å). By targeting lens cluster fields, a large sample of homogeneous, deep (with typical exposure times of $\sim$5 h), and high-resolution spectra of cluster galaxies, over a wide redshift range $0.3 < z < 0.9$, has been collected (Caminha et al. 2019, 2023; Bergamini et al. 2019, 2023a,b; Richard et al. 2021; Jauzac et al. 2021; Lagattuta et al. 2022). In addition, these MUSE observations allow for robust stellar velocity dispersion measurements, $\sigma_\star$, for statistically

significant samples of member galaxies (Bergamini et al. 2019, 2023a; Pignataro et al. 2021; Granata et al. 2022).

For instance, MACS 1149 has been observed with the VLT/MUSE instrument over an area of ~2 arcmin^2 with an exposure time of ~6 h (see Grillo et al. 2016, Schuldt et al., in prep.), resulting in the spectroscopic confirmation of 134 cluster member galaxies. In Fig. 2, we show a VLT/MUSE mean stacked spectrum of the 22 early-type cluster member galaxies with high stellar velocity dispersion values ($\sigma_\star > 180$ km s^{-1}) and characterised by a high signal-to-noise ratio ($S/N > 15$), showcasing the high S/N already achieved with a small sample. To create the stacked spectrum, we normalised the rest-frame shifted spectra of the selected galaxies by their median flux value in the rest-frame 4125–4275 Å wavelength range, where no prominent spectroscopic features are detected. The mean stacked spectrum has been smoothed with a Gaussian kernel with a standard deviation of 3.75 Å, allowing for a better visualisation of the spectral features. The resulting spectrum is representative of an old, massive, and passively evolving galaxy population, as suggested by the red continuum, the absence of emission lines (their expected positions are identified in blue), and the presence of several absorption lines (marked in red) or spectral features (such as the 4000 Å break) that are commonly used to estimate their age. In addition, some key Fe and Mg absorption features (Vazdekis et al. 2010), marked in green, can help estimate the metallicity of the stellar population and, thus, control the intrinsic age-metallicity degeneracy (see Moresco et al. 2022). Finally, to measure the value of dt (see Eq. (3)) at the effective redshift of MACS 1149 ($z_d = 0.54$), we can exploit already available VLT/MUSE observations of other lens clusters in close-by redshift bins such as SDSS J1029+2623 ($z = 0.59$) and SDSS J2222+2745 ($z = 0.49$). Within the single VLT/MUSE pointings of these cluster cores (Acebron et al. 2022a,b), 9 and 8 galaxies with $\sigma_\star > 180$ km s^{-1} have been identified, respectively. Their resulting mean stacked spectra are also shown in Fig. 2. These are characterised by a high average S/N, similar to that reported in previous studies (Stern et al. 2010a; Moresco et al. 2016; Borghi et al. 2022a, priv. comm.). We plan to exploit the extensive, high-quality VLT/MUSE spectroscopic coverage already available for several lens clusters, enabling the selection of a high-purity sample of optimal CCs to ultimately apply the newly proposed joint method.

5. Conclusions

In this work, we present a novel technique to boost and complement the power of time-delay cosmography in lens galaxy clusters by probing their member galaxies as pure samples of CCs, allowing for an independent measurement of the value of the Hubble parameter at the effective lens cluster redshift.

Considering as reference the well-studied lens galaxy cluster MACS J1149.5+2223, with the multiply-imaged SN 'Refsdal', we have assessed the complementarity of the two probes and quantified the achieved precision on the values of the relevant cosmological parameters through their combination. We have demonstrated that the estimate of the value of the Hubble constant is robust, depending only mildly on the chosen cosmological model. Since the two probes produce confidence regions on the cosmological parameter planes that are oriented in complementary ways, we have shown that their combination provides more precise measurements of the values of the other cosmological parameters. Finally, we discuss the immediate observational feasibility of the proposed joint method by exploiting the already
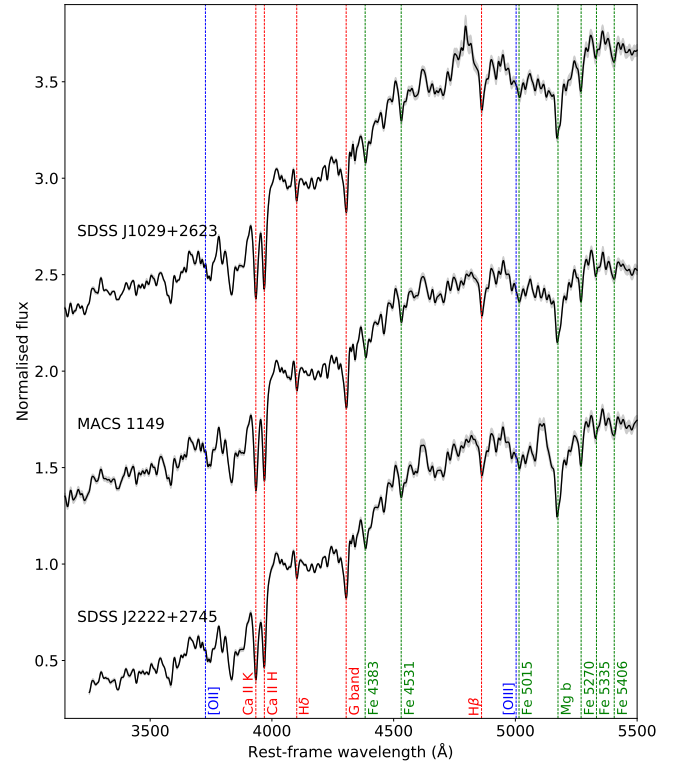
Fig. 2. VLT/MUSE mean stacked spectra of 9, 22, and 8 cluster member galaxies of SDSS J1029+2623 (top, $z = 0.59$), MACS 1149 (middle, $z = 0.54$), and SDSS J2222+2745 (bottom, $z = 0.49$), respectively, with $\sigma_\star > 180$ km s^{-1}. The shaded regions are the standard deviation of each spectral pixel. The spectra are smoothed by applying a Gaussian kernel with a standard deviation of 3.75 Å. For a clear visualisation, the flux values of MACS 1149 and SDSS J1029+2623 have been increased by 1 and 2, respectively. The red dashed vertical lines locate the absorption features detected in the spectra, while the blue lines mark the expected positions of emission lines characteristic of young, star-forming populations. The green dashed lines denote the Fe and Mg lines typically used to estimate the stellar metallicity of the population. We note that the strong residual emissions observed at 4800 Å and 5100 Å for SDSS J1029+2623 and SDSS J2222+2745, respectively, are due to an incomplete subtraction of sky lines.

available high-quality spectro-photometric data. These are necessary to select pure samples of cluster members as CCs and measure their ages for several cluster strong lensing systems.

Thanks to upcoming facilities such as the Legacy Survey of Space and Time, operated by the *Vera C. Rubin* Observatory, and such space missions as *Euclid* and JWST, a notable increase of known strong lensing clusters with time variable sources is expected. This will allow us to exploit them in combination with CCs as powerful cosmological probes.

References

Acebron, A., Grillo, C., Bergamini, P., et al. 2022a, A&A, 668, A142
Acebron, A., Grillo, C., Bergamini, P., et al. 2022b, ApJ, 926, 86
Acebron, A., Schuldt, S., Grillo, C., et al. 2023, A&A, 680, L9
Astropy Collaboration (Robitaille, T. P., et al.) 2013, A&A, 558, A33
Astropy Collaboration (Price-Whelan, A. M., et al.) 2018, AJ, 156, 123
Bacon, R., Accardo, M., Adjali, L., et al. 2012, The Messenger, 147, 4
Bergamini, P., Rosati, P., Mercurio, A., et al. 2019, A&A, 631, A130
Bergamini, P., Acebron, A., Grillo, C., et al. 2023a, A&A, 670, A60
Bergamini, P., Grillo, C., Rosati, P., et al. 2023b, A&A, 674, A79
Bernardi, M., Renzini, A., da Costa, L. N., et al. 1998, ApJ, 508, L143
Birrer, S., Treu, T., Rusu, C. E., et al. 2019, MNRAS, 484, 4726
Borghi, N., Moresco, M., & Cimatti, A. 2022a, ApJ, 928, L4
Borghi, N., Moresco, M., Cimatti, A., et al. 2022b, ApJ, 927, 164
Caminha, G. B., Grillo, C., Rosati, P., et al. 2016, A&A, 587, A80
Caminha, G. B., Grillo, C., Rosati, P., et al. 2017, A&A, 607, A93
Caminha, G. B., Rosati, P., Grillo, C., et al. 2019, A&A, 632, A36
Caminha, G. B., Suyu, S. H., Grillo, C., & Rosati, P. 2022, A&A, 657, A83
Caminha, G. B., Grillo, C., Rosati, P., et al. 2023, A&A, 678, A3
Cappellari, M. 2023, MNRAS, 526, 3273
Cerulo, P., Couch, W. J., Lidman, C., et al. 2016, MNRAS, 457, 2209
Courbin, F., Bonvin, V., Buckley-Geer, E., et al. 2018, A&A, 609, A71
De Lucia, G., Poggianti, B. M., Aragón-Salamanca, A., et al. 2007, MNRAS, 374, 809
Estrada, N., Mercurio, A., Vulcani, B., et al. 2023, A&A, 671, A146
Faber, S. M., Dressler, A., Davies, R. L., et al. 1987, Nearly Normal Galaxies. From the Planck Time to the Present, 175
Ferré-Mateu, A., Sánchez-Blázquez, P., Vazdekis, A., & de la Rosa, I. G. 2014, ApJ, 797, 136
Foreman-Mackey, D. 2016, J. Open Source Software, 1, 24
Foreman-Mackey, D., Hogg, D. W., Lang, D., & Goodman, J. 2013, PASP, 125, 306
Gladders, M. D., & Yee, H. K. C. 2000, AJ, 120, 2148
Gobat, R., Rosati, P., Strazzullo, V., et al. 2008, A&A, 488, 853
Goodman, J., & Weare, J. 2010, Commun. Appl. Math. Comput. Sci., 5, 65
Granata, G., Mercurio, A., Grillo, C., et al. 2022, A&A, 659, A24
Grillo, C., Karman, W., Suyu, S. H., et al. 2016, ApJ, 822, 78
Grillo, C., Rosati, P., Suyu, S. H., et al. 2018, ApJ, 860, 94
Grillo, C., Rosati, P., Suyu, S. H., et al. 2020, ApJ, 898, 87
Harris, C. R., Millman, K. J., van der Walt, S. J., et al. 2020, Nature, 585, 357–362
Hilton, M., Stanford, S. A., Stott, J. P., et al. 2009, ApJ, 697, 436
Hunter, J. D. 2007, Comput. Sci. Eng., 9, 90
Jauzac, M., Klein, B., Kneib, J.-P., et al. 2021, MNRAS, 508, 1206
Jimenez, R., & Loeb, A. 2002, ApJ, 573, 37
Jullo, E., Natarajan, P., Kneib, J. P., et al. 2010, Science, 329, 924
Kelly, P. L., Rodney, S. A., Treu, T., et al. 2015, Science, 347, 1123
Kelly, P. L., Brammer, G., Selsing, J., et al. 2016, ApJ, 831, 205
Kelly, P. L., Rodney, S., Treu, T., et al. 2023, ApJ, 948, 93
Khullar, G., Bayliss, M. B., Gladders, M. D., et al. 2022, ApJ, 934, 177
Lagattuta, D. J., Richard, J., Bauer, F. E., et al. 2022, MNRAS, 514, 497
Lagattuta, D. J., Richard, J., Ebeling, H., et al. 2023, MNRAS, 522, 1091
Lidman, C., Rosati, P., Tanaka, M., et al. 2008, A&A, 489, 981
Linder, E. V. 2011, Phys. Rev. D, 84, 123529
Lotz, J. M., Koekemoer, A., Coe, D., et al. 2017, ApJ, 837, 97
Menci, N., Rosati, P., Gobat, R., et al. 2008, ApJ, 685, 863
Millon, M., Courbin, F., Bonvin, V., et al. 2020, A&A, 640, A105
Moresco, M. 2015, MNRAS, 450, L16
Moresco, M., Cimatti, A., Jimenez, R., et al. 2012, J. Cosmol. Astropart. Phys., 2012, 006
Moresco, M., Pozzetti, L., Cimatti, A., et al. 2016, J. Cosmol. Astropart. Phys., 2016, 014
Moresco, M., Amati, L., Amendola, L., et al. 2022, Liv. Rev. Relativ., 25, 6
Pignataro, G. V., Bergamini, P., Meneghetti, M., et al. 2021, A&A, 655, A81
Postman, M., Coe, D., Benítez, N., et al. 2012, ApJS, 199, 25
Ratsimbazafy, A. L., Loubser, S. I., Crawford, S. M., et al. 2017, MNRAS, 467, 3239
Refsdal, S. 1964, MNRAS, 128, 307
Richard, J., Claeyssens, A., Lagattuta, D., et al. 2021, A&A, 646, A83
Shajib, A. J., Mozumdar, P., Chen, G. C. F., et al. 2023, A&A, 673, A9
Simon, J., Verde, L., & Jimenez, R. 2005, Phys. Rev. D, 71, 123001
Stern, D., Jimenez, R., Verde, L., Kamionkowski, M., & Stanford, S. A. 2010a, J. Cosmol. Astropart. Phys., 2010, 008
Stern, D., Jimenez, R., Verde, L., Stanford, S. A., & Kamionkowski, M. 2010b, ApJS, 188, 280
Strazzullo, V., Daddi, E., Gobat, R., et al. 2016, ApJ, 833, L20
Suyu, S. H., Marshall, P. J., Auger, M. W., et al. 2010, ApJ, 711, 201
Suyu, S. H., Treu, T., Hilbert, S., et al. 2014, ApJ, 788, L35
Suyu, S. H., Bonvin, V., Courbin, F., et al. 2017, MNRAS, 468, 2590
Thomas, D., Maraston, C., Bender, R., & Mendes de Oliveira, C. 2005, ApJ, 621, 673
Treu, T., & Marshall, P. J. 2016, A&ARv, 24, 11
Treu, T., Ellis, R. S., Liao, T. X., et al. 2005, ApJ, 633, 174
Treu, T., Brammer, G., Diego, J. M., et al. 2016, ApJ, 817, 60
van der Walt, S., Colbert, S. C., & Varoquaux, G. 2011, Comput. Sci. Eng., 13, 22
Van Rossum, G., & Drake, F. L. 2009, Python 3 Reference Manual (Scotts Valley, CA: CreateSpace)
Vazdekis, A., Sánchez-Blázquez, P., Falcón-Barroso, J., et al. 2010, MNRAS, 404, 1639
Verde, L., Treu, T., & Riess, A. G. 2019, Nat. Astron., 3, 891
Virtanen, P., Gommers, R., Oliphant, T. E., et al. 2020, Nature Methods, 17, 261
Wolz, L., Kilbinger, M., Weller, J., & Giannantonio, T. 2012, J. Cosmol. Astropart. Phys., 2012, 009
Wong, K. C., Suyu, S. H., Chen, G. C. F., et al. 2020, MNRAS, 498, 1420
Zhang, C., Zhang, H., Yuan, S., et al. 2014, Res. Astron. Astrophys., 14, 1221